A comparative study of various CBCT reconstruction methods for sparsely sampled projection data

Jonghee Yun [a], Seungwoo Ha [a], Ho Kyung Kim [a,b*]
[a]*School of Mechanical Engineering, Pusan National University, Busan, South Korea*
[b]*Center for Advanced Mechanical Engineering Research, Pusan National University, Busan, South Korea*
[*]*Corresponding author: hokyung@pusan.ac.kr*

1. Introduction

To obtain high-quality CT images, a large number of projection data must be acquired. However, patients are exposed to large amounts of x-rays, which can increase the potential risk of cancer. In dental CT, low-dose CT scan is might be important because x-rays can be absorbed in important organs such as the brain and eyes. Many methods for acquiring high-quality CT images while exposing small amount of x-rays have been proposed [1-3]. One of them is to acquire a small number of projection data and reconstruct images with them. When the image reconstruction is performed with a small number of projection data using filtered backprojection (FBP), which is an analytic algorithm widely used for image reconstruction, streak artifacts occur and quality of reconstructed images becomes worse. Unlike the FBP, it is possible to obtain reconstructed images with reduced artifacts and noise even with a small number of projection data by using iterative image reconstruction methods. Iterative image reconstruction methods include simultaneous algebraic reconstruction technique (SART), maximum-likelihood expectation-maximization (MLEM), model-based iterative reconstruction (MBIR), and compressed sensing (CS).

We compare the performance of various reconstruction methods for sparsely sampled projection data using image quality indexes. The image reconstruction algorithms used in this study are FBP, SART, MLEM and CS-based total-variation (TV) minimization.

2. Materials and Methods

2.1 Filtered Backprojection

The FBP algorithm is the most commonly used algorithm for CBCT image reconstruction. Since it analytically calculate slice images, it can provide accurate and fast reconstructed images. The FBP algorithm approximates the backprojection procedure of cone beam geometry to parallel beam geometry. Through a given depth *z* the image plane (*x*, *y*) reconstructed by the FBP algorithm can be expressed as [4]

$$f(x,y)=\int_0^{2\pi}\frac{d_{\mathrm{SA}}^2}{\left(d_{\mathrm{SA}}-s\right)^2}\int_{-\infty}^{\infty}p'_{\beta}(\xi,\eta)h(\xi'-\xi)\mathrm{d}\xi\mathrm{d}\beta\,, \quad (1)$$

where β refers to the projection angle, d_{SA} refer to the source-to-AOR distance, s is the distance of a voxel from a virtual detector plane moved to the AOR, (ξ,ζ) represents the pixel coordinates in the detector plane, $p_{\beta}'(\xi,\eta)$ is the projection image multiplied by cosine weighting factor, and $h(\cdot)$ is the reconstruction filter function.

2.2 Simultaneous algebraic reconstruction technique

However, when reconstructing the image using the FBP algorithm with sparsely sampled projection data, streak artifacts occur in the reconstructed images. However, if the image reconstruction is performed with the iterative reconstruction algorithm, reconstructed images with reduced artifacts and noise can be obtained compared with the FBP even with sparsely sampled projection data. The SART is one of the most commonly used iterative reconstruction algorithm. The SART estimates the reconstructed image by updating the previous pixel values considering the differences between the measurements and the numerical computations. A 3D image is updated with the SART algorithm by using the following formation [5]

$$f_j^{(i+1)}=f_j^{(i)}+\frac{1}{\sum_i a_{ij}}\sum_i\left[a_{ij}\frac{p_i-a_i^T f^{(i)}}{\sum_{j=1}^{N}a_{ij}}\right], \quad (2)$$

where i denotes the index of iteration and a_{ij} describes the projection of the jth pixel by the ith ray, and p_i is measured projection data.

2.3 Maximum-likelihood expectation-maximization

The SART algorithm is a method of setting up the difference between measured projection data and calculated projection data as an objective function and iteratively minimizing it. On the other hand, the MLEM algorithm is a method to minimize the different objective function by using the Poisson noise model and the non-negativity constraint. The MELM calculates the reconstructed image considering the ratio of the measured projection data to the calculated projection data instead of difference. A 3D reconstructed image with the MLEM algorithm can be represented with [6]

$$f_j^{(i+1)} = \frac{f_j^{(i)}}{\sum_i a_{ij}} \sum_i \left[a_{ij} \frac{p_i}{\sum_{j=1}^{N} a_{ij} f^{(i)}} \right]. \quad (3)$$

2.4 Total-variation minimization

A method of iteratively reconstructing the image by using a CS technique was proposed to reconstruct an image accurately even with insufficient projection data. In medical and other applications, rapid variation in the image may only occur at boundaries of internal structures. Thus, the CS technique makes an assumption that an image itself might not be sparse, but its gradient image could be approximately sparse [7]. The CS-based TV minimization algorithm sets up a discrete linear system. To solve the linear system, TV minimization algorithm is performed by the gradient descent method and projection onto convex sets. The TV minimization algorithm can be expressed as follow [7,8]:

$$\min \left\| \vec{f} \right\|_{TV}, \text{ such that } \vec{g} = M\vec{f} . \quad (4)$$

An purpose of TV minimization algorithm is to minimize the $l_1 - \text{norm}$ of the gradient image, known as the TV of the image. The TV minimization is known to reduce noise and preserve edges in the images. The TV of image can be described by the following equation:

$$\left\| \vec{f} \right\|_{TV} = \sum_{x,y,z} \sqrt{(\nabla_x f)^2 + (\nabla_y f)^2 + (\nabla_z f)^2} . \quad (5)$$

2.5 Image quality evaluation metrics

We use structural similarity (SSIM), mutual information (MI), root mean square error (RMSE), and streak indicator (SI) as image quality evaluation metrics to numerically compare the image quality of reconstructed images with various algorithms.

The SSIM is commonly used for comparing two images in terms of the means and standard deviations of corresponding pixel values as well as their covariance. The SSIM is given by [9]

$$\text{SSIM}(x,y) = \frac{(2\mu_x\mu_y + C_1)(2\sigma_{xy} + C_2)}{(\mu_x^2 + \mu_y^2 + C_1)(\sigma_x^2 + \sigma_y^2 + C_2)}, \quad (6)$$

where μ_x and μ_y are the average of x and y, respectively. σ_x^2 and σ_y^2 are the variance of x and y, respectively. σ_{xy} is the covariance of x and y. And C_1 and C_2 are variables to stabilize the division with weak denominator, which is defined as $(k_1 L)^2$ and $(k_2 L)^2$, respectively, where L is the dynamic range of the pixel-values, and k_1 and k_2 are 0.01 and 0.03 by default, respectively.

The MI measures the mutual dependence between the two images. The MI can be defined by [10]

$$I(X;Y) = \sum_{y \in Y} \sum_{x \in X} p(x,y) \log_2 \left(\frac{p(x,y)}{p(x)p(y)} \right), \quad (7)$$

where $p(x,y)$ is the joint probability function of x and y, and $p(x)$ and $p(y)$ are the marginal probability distribution function of x and y, respectively.

The RMSE value is suitable for representing the precision by measuring the difference the two images. It is also indicates how far apart the individual measurements are from the mean value. The RMSE is defined by

$$\text{RMSE}(x,y) = \sqrt{\frac{\sum_{i,j} \left(x_{i,j} - y_{i,j} \right)^2}{N}}, \quad (8)$$

where i and j are the pixel index of the row and column, respectively, and N is the total number of pixels.

In order to quantify the under-sampling streak artifacts, the metric SI based on the TV values of an image is introduced. The SI is can be expressed as [11]

$$\text{SI} = \text{TV}\left(I - I_{ref} \right), \quad (9)$$

where I and I_{ref} are reconstructed image and reference image, respectively. The original image or many views of FBP image are used as reference image. A larger TV value corresponds to stronger streak artifacts. When the metric SI is interpreted in results, the relative change of SI values is more important than the absolute SI values.

3. PRELIMINARY RESULT

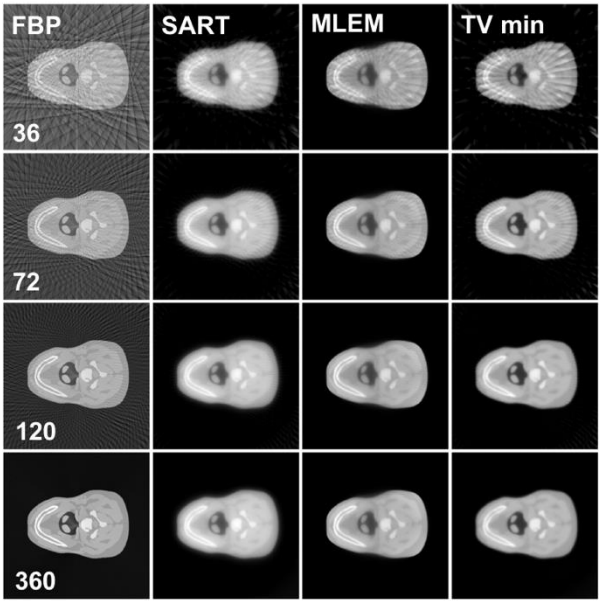

Fig. 1. Reconstructed slice images of XCAT phantom by using the four reconstruction algorithms. The images in each column are obtained by FBP, SART, MLEM, and TV minimization. The images of each row are obtained by 36, 72, 120, 360 projections.

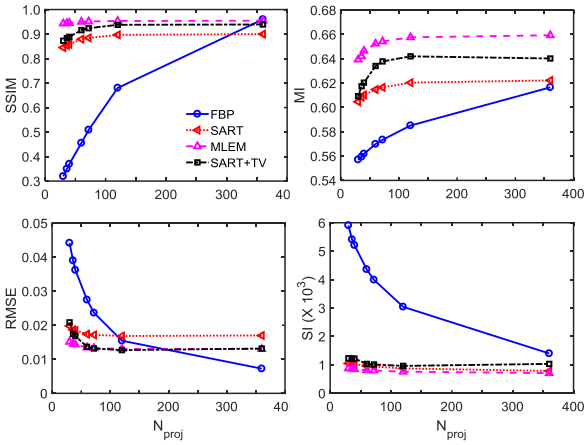

Fig. 2. The image quality evaluation metrics for the number of projections.

Fig. 1 shows the reconstructed images of XCAT phantoms obtained by using the four reconstruction algorithms. The images of each row are obtained as 36, 72, 120, and 360 projection images, respectively, and the images of each column are reconstructed by FBP, SART, MLEM, and TV minimization, respectively.

Fig. 2 shows the image quality evaluation metrics for the number of projections in order to determine the similarity between the original image and the reconstructed images acquired by using four image reconstruction algorithms. The results of the FBP were worst except for using 360 projections, and the results of the MLEM and TV minimization are the best among the four image reconstruction algorithms.

4. FURTHER STUDY

The simulation study was performed with various image reconstruction algorithms. We will experimentally obtain projection data, perform image reconstruction with various algorithms and compare the results.

ACKNOWLEDGEMENT

This work was supported by the National Research Foundation of Korea (NRF) grant funded by the Korea government (MSIP) (No. 2017M2A2A6A01071267).

REFERENCES

[1] E. Y. Sidky, and X. Pan, Image reconstruction in circular cone-beam computed tomography by constrained, total-variation minimization, *Phys. Med. Biol.*, Vol. 53, no. 17, pp. 4777, 2008.
[2] X. Han, J. Bian, E. L. Ritman, E. Y. Sidky, and X. Pan, Optimization-based reconstruction of sparse images from few-view projections, *Phys. Med. Biol.*, Vol. 57, no. 16, pp. 5245, 2012.
[3] G. H. Chen, J. Tang, and S. Leng, Prior image constrained compressed sensing (PICCS): a method to accurately reconstruct dynamic CT images from highly undersampled projection data sets,
[4] L. A. Feldkamp, L. C. Davis, and J. W. Kress, Practical cone-beam algorithm, *J. Opt. Soc. Am. A.*, Vol. 1, pp. 612-619, 1984.
[5] A. C. Kak and M. Slaney, Principles of computed tomography imaging, IEEE press, New York, 1988.
[6] K. Lange and R. Carson, EM reconstruction algorithms for emission and transmission tomography, *J. Comput. Assist. Tomogr.*, Vol. 8, no. 2, pp. 306-316, 1984.
[7] E. J. Candes, J. Romberg, and T. Tao, Robust uncertainty principles: Exact signal reconstruction from highly incomplete frequency information, *IEEE T. Inform. Theory*, Vol. 52, no. 2, pp. 489-509, 2006.
[8] E. Y. Sidky, C. M. Kao, and X. Pan, Accurate image reconstruction from few-views and limited-angle data in divergent-beam CT, *J. X-ray Sci. Technol.*, Vol. 14, no. 2, pp. 119-139, 2006.
[9] Z. Wang, A. C. Bovik, H. R. Sheikh, E. P. Simoncelli, Image quality assessment: From error measurement to structural similarity, IEEE Trans. Image Process., vol. 13, no. 4, pp. 600-512, Apr. 2004.
[10] Cover, Thomas M., and Joy A. Thomas. Elements of information theory. John Wiley & Sons, 2012.
[11] J. Tang, E. N. Brian, and G. H. Chen, Performance comparison between total variation (TV)-based compressed sensing and statistical iterative reconstruction algorithms, *Phys. Med. Biol.*, Vol. 54, no. 19, pp. 5781, 2009.